

Supporting Information

Novel zinc-iodine hybrid supercapacitors with boosted energy density using redox iodide ion electrolyte and B, N dual doped carbon electrode

Lu Han^{a&}, Hailong Huang^{a&}, Junfeng Li^a, Zhongli Yang^a, Xinlu Zhang^a, Dafeng Zhang^b, Xinjuan Liu^c, Min Xu^{a*} and Likun Pan^{a*}

^a School of Physics and Materials Science & Shanghai Key Laboratory of Magnetic Resonance, East China Normal University, No. 3663 North Zhongshan Road, Shanghai 200062, P R China.

^b School of Materials Science and Engineering, Liaocheng University, Liaocheng, Shandong 252000, PR China.

^c Institute of Optoelectronic Materials and Devices, College of Optical and Electronic Technology, China Jiliang University, Hangzhou, 310018, China.

Fax: +86 21 62234321; Tel: +86 21 62234132; E-mail: lkpan@phy.ecnu.edu.cn;

Fax: +86 21 62233281; Tel: + 86 21 62233263; E-mail: xumin@phy.ecnu.edu.cn.

Experimental section

Characterizations

The morphologies and structures of the samples were measured by scanning electron microscopy (SEM) (JSM 7500F, JEOL), transmission electron microscopy (TEM), and high-resolution TEM (HR-TEM, JEM 2010 JEOL). The specific surface area and pore size distribution were determined by an ASAP 2020 Accelerated Surface Area and Porosimetry System (V-Sorb 2800P). X-ray diffraction (XRD) pattern was recorded by X-ray diffractometer (Holland Panalytical PRO PW 3040/60, $V = 35$ kV, $I = 25$ mA, $\lambda = 1.5418$ Å). X-ray photoelectron spectroscopy (XPS) measurement was carried out on a Thermo ESCALAB 250XI. Raman spectrum was collected on a Renishaw Raman spectrometer with a laser wavelength of 488 nm at room temperature.

Electrochemical Measurements.

The carbon-based electrodes were prepared by coating a homogenous slurry of BN-CMT or N-CMT powder, carbon black (Super-P) and polyvinylidene fluoride (adhesive agent) in N-methylpyrrolidone solvent with a weight ratio of 80 : 10 : 10 onto graphite substrates, and then dried at 60 °C for 24 h in the constant temperature oven. Typically, each working electrode has an exposed area of 1×1 cm² and an active material mass loading of 1 mg. Zn metal foil was

directly used as anode, which should be polished with finegrained sandpaper to avoid being oxidized. The redox-active electrolyte was prepared by adding 0.001 mol zinc iodide (ZnI_2) into 100 mL 1 M ZnSO_4 aqueous electrolyte without separating the anolyte and catholyte. Cyclic voltammetry (CV), galvanostatic charge-discharge (GCD), and electrochemical impedance spectroscopy (EIS) tests were conducted using an electrochemical workstation (Autolab PGSTAT302N). The cycling stability measurement of zinc-iodine hybrid supercapacitors (Z-IHS) was carried out on a LAND battery-testing instrument with a sweep charge and discharge rate at 10 A g^{-1} for 10000 cycles.

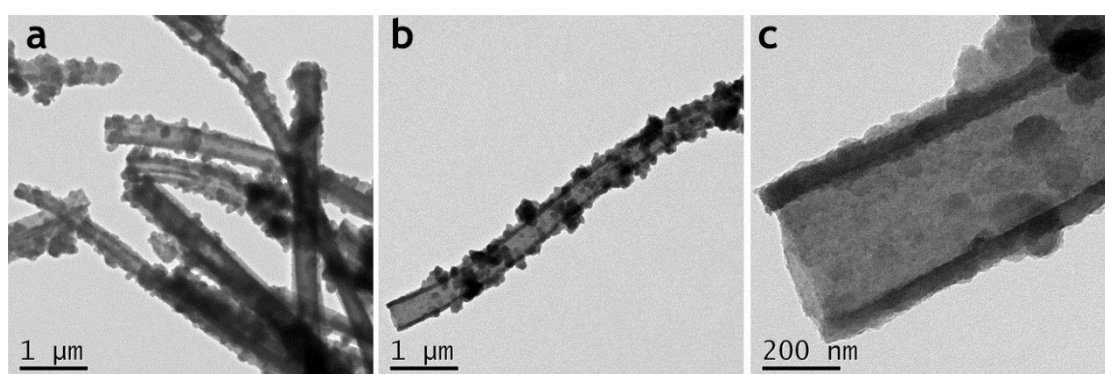


Fig. S1 (a-c) TEM images of BN-CMT.

Table S1 Specific surface areas, mean pore diameters, pore volumes and of N-CMT and BN-CMT.

Sample	Specific surface area ($\text{m}^2 \text{ g}^{-1}$)	Mean pore diameter (nm)	Pore volume ($\text{cm}^3 \text{ g}^{-1}$)
N-CMT	76.72	3.41	0.19

BN-CMT 101.24 3.05 0.23

Table S2 Contents of B, N, C, and O in N-CMT and BN-CMT determined from XPS elemental analysis.

Sample	B (at. %)	N (at. %)	C (at. %)	O (at. %)
N-CMT	0%	12.07%	84.05%	3.88%
BN-CMT	7.33%	14.25%	68.74%	9.69%

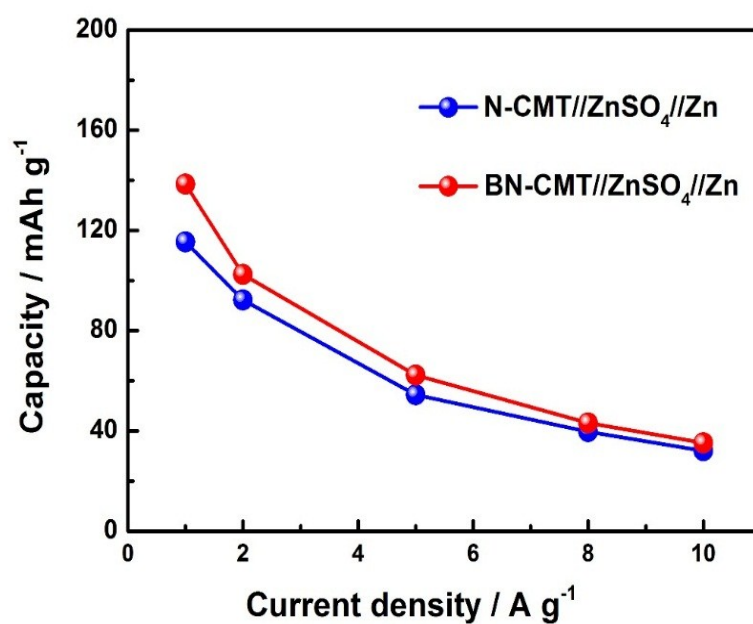


Fig. S2 Specific capacities of N-CMT and BN-CMT as a function of discharge current density in ZHS.

Table S3 Charge-transfer resistances of N-CMT and BN-CMT in different electrolytes.

Sample	R_{ct} (Ω) in 1 M $ZnSO_4$ electrolyte	R_{ct} (Ω) in 1 M $ZnSO_4$ + 0.01 M ZnI_2 electrolyte
N-CMT	0.92	0.46
BN-CMT	0.58	0.16

Table S4 Discharge specific capacities of N-CMT and BN-CMT in ZHS at current densities of 1-10 $A\ g^{-1}$.

Current density ($A\ g^{-1}$)	1	2	5	8	10
N-CMT (ZHS, $mAh\ g^{-1}$)	115.5	92.3	54.4	39.6	32
BN-CMT (ZHS, $mAh\ g^{-1}$)	138.5	102.5	62.2	43.2	35.2

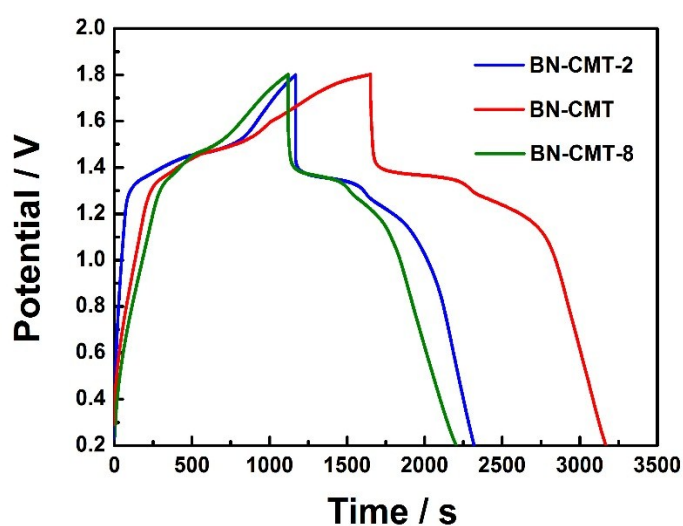


Fig. S3 GCD curves of BN-CMT-2, BN-CMT and BN-CMT-8 in Z-IHS.

Table S5 Discharge specific capacities of BN-CMT-2, BN-CMT and BN-CMT-8 in Z-IHS at current densities of 1-10 A g⁻¹.

Current density (A g ⁻¹)	1	2	5	8	10
BN-CMT-2 (Z-IHS, mAh g⁻¹)	319.7	191.1	90.7	59.4	46.9
BN-CMT (Z-IHS, mAh g⁻¹)	416.6	222.9	122.3	86.2	70.3
BN-CMT-8 (Z-IHS, mAh g⁻¹)	300.8	196.8	117.6	81.1	67.2

Table S6 Comparison of electrochemical performances of BN-CMT based Z-HIS with the conventional ZHS reported in the literatures.

Electrode material	Specific capacity / capacitance	Electrolyte	Energy density (Wh kg ⁻¹)	Operating voltage window (V)	Ref.
Zn//BN-CMT	416.6 mAh g ⁻¹	1 M ZnSO ₄ + 0.01 M ZnI ₂ (aqueous)	472.6	0.2-1.8	This work
Zn//AC	170 F g ⁻¹	1 M Zn (CF ₃ SO ₃) ₂ (organic)	52.7	0-1.8	[1]
Zn//AC	121 mAh g ⁻¹	2 M ZnSO ₄ (aqueous)	84	0.2-1.8	[2]
Zn//graphene@polyaniline	154 mAh g ⁻¹	2 M ZnSO ₄ (aqueous)	205	0.3-1.6	[3]
Zn//MXene-graphene aerogel	128.6 F g ⁻¹	2 M ZnSO ₄ (aqueous)	34.9	0.2-1.6	[4]
Zn//AC	/	2 M ZnSO ₄ (aqueous)	94	0.2-1.8	[5]
Zn//Carbon spheres	86.8 mAh g ⁻¹	ZnSO ₄ gel electrolyte	59.7	0.15-1.95	[6]
Zn@Ti ₃ C ₂ // Ti ₃ C ₂	132 F g ⁻¹	ZnSO ₄ gel electrolyte	/	0.1-1.35	[7]

References

- [1] H. Wang, M. Wang and Y. Tang, *Energy Storage Mater.*, 2018, **13**, 1-7.
- [2] L. Dong, X. Ma, Y. Li, L. Zhao, W. Liu, J. Cheng, C. Xu, B. Li, Q.-H. Yang and F. Kang, *Energy Storage Mater.*, 2018, **13**, 96-102.
- [3] J. Han, K. Wang, W. Liu, C. Li, X. Sun, X. Zhang, Y. An, S. Yi and Y. Ma, *Nanoscale*, 2018, **10**, 13083-13091.
- [4] Q. Wang, S. Wang, X. Guo, L. Ruan, N. Wei, Y. Ma, J. Li, M. Wang, W. Li and W. Zeng, *Adv. Electron. Mater.*, 2019, DOI: 10.1002/aelm.201900537.
- [5] L. He, Y. Liu, C. Li, D. Yang, W. Wang, W. Yan, W. Zhou, Z. Wu, L. Wang, Q. Huang, Y. Zhu, Y. Chen, L. Fu, X. Hou and Y. Wu, *ACS Appl. Energy Mater.*, 2019, **2**, 5835-5842.
- [6] S. Chen, L. Ma, K. Zhang, M. Kamruzzaman, C. Zhi and J. A. Zapien, *J. Mater. Chem. A*, 2019, **7**, 7784-7790.
- [7] Q. Yang, Z. Huang, X. Li, Z. Liu, H. Li, G. Liang, D. Wang, Q. Huang, S. Zhang, S. Chen and C. Zhi, *ACS Nano*, 2019, **13**, 8275-8283.